VEGFR2 Signaling Prevents Colorectal Cancer Cell Senescence to Promote Tumorigenesis in Mice With Colitis

Sebastian Foersch,[1] Tobias Sperka,[2] Christina Lindner,[1] Astrid Taut,[1] Karl L. Rudolph,[2] Georg Breier,[3] Frank Boxberger,[1] Tilman T. Rau,[4] Arndt Hartmann,[4] Michael Stürzl,[5] Nadine Wittkopf,[1] Lisa Haep,[5] Stefan Wirtz,[1] Markus F. Neurath,[1] and Maximilian J. Waldner[1]

[1]Department of Medicine 1, FAU Erlangen-Nürnberg, Erlangen, Germany; [2]Fritz Lipmann Institute, Leibniz Institute for Age Research, Jena, Germany; [3]Department of Pathology, Dresden University of Technology, Dresden, Germany; [4]Department of Pathology, FAU Erlangen-Nürnberg, Erlangen, Germany; and [5]Division of Molecular and Experimental Surgery, FAU Erlangen-Nürnberg, Erlangen, Germany

BACKGROUND & AIMS: Senescence prevents cellular transformation. We investigated whether vascular endothelial growth factor (VEGF) signaling via its receptor, VEGFR2, regulates senescence and proliferation of tumor cells in mice with colitis-associated cancer (CAC). **METHODS:** CAC was induced in VEGFR2$^{\Delta IEC}$ mice, which do not express VEGFR2 in the intestinal epithelium, and VEGFR2$^{fl/fl}$ mice (controls) by administration of azoxymethane followed by dextran sodium sulfate. Tumor development and inflammation were determined by endoscopy. Colorectal tissues were collected for immunoblot, immunohistochemical, and quantitative polymerase chain reaction analyses. Findings from mouse tissues were confirmed in human HCT116 colorectal cancer cells. We analyzed colorectal tumor samples from patients before and after treatment with bevacizumab. **RESULTS:** After colitis induction, VEGFR2$^{\Delta IEC}$ mice developed significantly fewer tumors than control mice. A greater number of intestinal tumor cells from VEGFR2$^{\Delta IEC}$ mice were in senescence than tumor cells from control mice. We found VEGFR2 to activate phosphatidylinositol-4,5-bisphosphate-3-kinase and AKT, resulting in inactivation of p21 in HCT116 cells. Inhibitors of VEGFR2 and AKT induced senescence in HCT116 cells. Tumor cell senescence promoted an anti-tumor immune response by CD8$^+$ T cells in mice. Patients whose tumor samples showed an increase in the proportion of senescent cells after treatment with bevacizumab had longer progression-free survival than patients in which the proportion of senescent tumor cells did not change before and after treatment. **CONCLUSIONS:** Inhibition of VEGFR2 signaling leads to senescence of human and mouse colorectal cancer cells. VEGFR2 interacts with phosphatidylinositol-4,5-bisphosphate-3-kinase and AKT to inactivate p21. Colorectal tumor senescence and p21 level correlate with patient survival during treatment with bevacizumab.

Keywords: Angiogenesis; Colon Cancer; Mouse Model; Inflammation.

Carcinogenesis of the colorectum is a multistep process that involves initiation, promotion, and, finally, progression into invasive carcinoma.[1,2] Recently, the vascular endothelial growth factor (VEGF) pathway moved to the center of attention during inflammation-associated colorectal carcinogenesis. Generally, VEGF is regarded as the key mediator of tumor angiogenesis.[3] The main effector is the VEGF receptor 2 (VEGFR2), which is expressed by endothelial cells (ECs). Activation of VEGFR2 on ECs results in their proliferation, migration, and increased survival.[4] Consequently, strategies blocking VEGF signaling were able to reduce tumor growth in multiple studies, which led to the approval of bevacizumab (anti-VEGF antibody) for the treatment of human cancer.[5]

Growing evidence supports the role of VEGF as an autocrine, paracrine, and even "intracrine" growth factor for tumor cells themselves, independent from its role in angiogenesis. Among others, this was studied for breast cancer cells,[6] skin cancer cells,[7] CD133$^+$ glioblastoma stem cells,[8] and in colitis-associated carcinogenesis.[9] Regarding colitis-associated cancer (CAC), we could show that VEGFR2 is up-regulated on intestinal epithelial cells (IECs) during acute and chronic inflammation, and its activation increases tumor promotion and proliferation. Although these results prompt VEGFR signaling to be an important molecular link between inflammation and colorectal cancer (CRC), details on the underlying mechanisms are scarce.

Using conditional knockout mice for VEGFR2 (VEGFR2$^{\Delta IEC}$) for the first time, we show that VEGF/VEGFR2 signaling plays a crucial role in inflammation-associated carcinogenesis by bypassing cellular senescence in IECs and promoting tumor development and progression. VEGFR2$^{\Delta IEC}$ mice were significantly protected against inflammatory carcinogenesis, and VEGFR2$^{\Delta IEC}$ tumors displayed a senescent phenotype. On the molecular

level, autocrine VEGF/VEGFR2 signaling in CRC cells seems to lead to an activation of the phosphatidylinositol-4,5-bisphosphate-3-kinase (PI3K)/AKT cascade, with subsequent inactivation and degradation of p21$^{WAF1/Cip1}$, a central molecule in senescence induction and maintenance (further referred to as p21). In addition, systemic VEGFR2 inhibition reduced tumor growth and enabled cellular senescence in experimental CAC. This effect was functionally dependent on both the induction of senescence and subsequent adaptive immune response. In addition, the ability to induce tumor cell senescence was associated with improved progression-free survival in bevacizumab-treated CRC patients.

Our findings highlight a central role of VEGF signaling independent from angiogenesis, and suggest an unknown connection between escape from aging-associated safeguard programs and inflammation-associated carcinogenesis.

Materials and Methods

Animal Models

Animal experiments were approved by the Institutional Animal Care and Use Committee of the State Government of Middle Franconia and conformed to national and international guidelines. VEGFR2$^{fl/fl}$ mice, Villin-Cre mice, and p21$^{-/-}$ mice have been described and were bred on a C57BL/6 background.[10–13] VEGFR2$^{fl/fl}$ mice were crossbred with Villin-Cre mice to generate VEGFR2$^{\Delta IEC}$ mice lacking the VEGFR2 in their IECs. All animals used were 8- to 10-week-old females (if not indicated otherwise). Azoxymethane (AOM)+dextran sodium sulfate (DSS) colorectal carcinogenesis was induced as described previously.[14]

Endoscopy, Narrow-Band Imaging, and Full-Body Fluorescence Imaging

High-definition endoscopy was achieved using specialized endoscopes, which have been described recently by our group.[15] Severity of colitis, tumor count, and tumor mass were determined using an established endoscopic scoring system.[16] Narrow-band imaging was used for vessel characterization.

Senescence-Associated β-Galactosidase Assay

Senescence-associated β-galactosidase (Sen-β-Gal) staining was performed using the Cell Signaling staining kit with a modified protocol (Cell Signaling Technology, Danvers, MA). Briefly, for tissue staining, colonic and tumorous tissues were removed, snap frozen in liquid nitrogen, and cryosectioned within 15 minutes after removal. Sen-β-Gal solution adjusted for pH 6 and the tissue was incubated overnight at 37°C.

Administration of Vascular Endothelial Growth Factor Receptor 2 Inhibitor, CD8$^+$ Depletion Antibody

Treatment of C57BL/6 and p21$^{-/-}$ mice with VEGFR2 inhibitors, CD8$^+$ T-cell depletion was initiated after endoscopic detection of already established tumors at week 4 of the AOM+DSS protocol.

Results

Loss of Vascular Endothelial Growth Factor Receptor 2 Signaling in Intestinal Epithelial Cells Protects Against Tumor Development in an Experimental Model of Colitis-Associated Cancer

To investigate the functional role and the underlying molecular mechanisms of VEGFR2 signaling in CAC, we generated a conditional knockout for this receptor in IECs by crossbreeding mice with floxed VEGFR2 alleles and mice expressing the Cre-recombinase under the control of the intestinal villin promoter (referred to as VEGFR2$^{\Delta IEC}$; Figure 1A). Specific deletion of VEGFR2 was confirmed by quantitative polymerase chain reaction (qPCR) of IEC complementary DNA after inflammatory challenge with DSS (Supplementary Figure 1A). Immunofluorescence staining revealed a lack of receptor expression in IECs when compared with VEGFR2$^{fl/fl}$ mice (control, Figure 1B). Endoscopy of VEGF2$^{\Delta IEC}$ mice revealed no spontaneous phenotype in the lower gastrointestinal tract, which was confirmed by histology (Supplementary Figure 1B).

To induce colitis-associated tumor development, VEGFR2$^{\Delta IEC}$ and matched VEGFR2$^{fl/fl}$ control mice were exposed to AOM+DSS (Figure 1C).[17,18] Colonoscopy was performed to evaluate different tumor parameters and the severity of intestinal inflammation.[16] VEGFR2$^{\Delta IEC}$ mice showed significantly fewer tumors and a significantly lower tumor load, as compared with control mice. Mean tumor size also differed, but did not reach statistical significance (Figure 1D).

Previous studies had suggested that the absence of VEGF reduces the severity of intestinal inflammation in an acute model of colitis and therefore might influence tumor development.[19] However, there was no significant difference in endoscopic activity of chronic DSS colitis between VEGFR2$^{\Delta IEC}$ and control mice (Figure 1E). We further investigated levels of oxidative stress as a possible initiator of tumor development. Immunohistochemistry (IHC) for the surrogate marker 8-hydroxydesoxyguanosine showed an increase in inflamed colonic tissue when compared with healthy control tissue from control mice (Figure 2A). This was further demonstrated by full-body fluorescence imaging using a fluorescent probe for reactive oxygen species detection (ROS Brite 700 nm; AAT Bioquest, Sunnyvale, CA) (Figure 2B). However, there was no difference in mucosal 8-hydroxydesoxyguanosine expression between VEGFR2$^{\Delta IEC}$ and control mice.

As these findings excluded the possibility that the differences in tumorigenesis between VEGFR2$^{\Delta IEC}$ and control mice were due to changes in colitis activity, we assessed the role of angiogenesis.[4] We performed CD31 staining of tumor tissue of both groups and calculated microvessel density (MVD). No differences in MVD could be observed. Likewise, narrow-band imaging endoscopy and full-body fluorescence imaging studies using a vessel-specific fluorescent probe (αVβ3-integrin) showed no difference in overall macroscopic vascularity (Figure 2C and D). We concluded that differences in tumor development, growth, and morphology
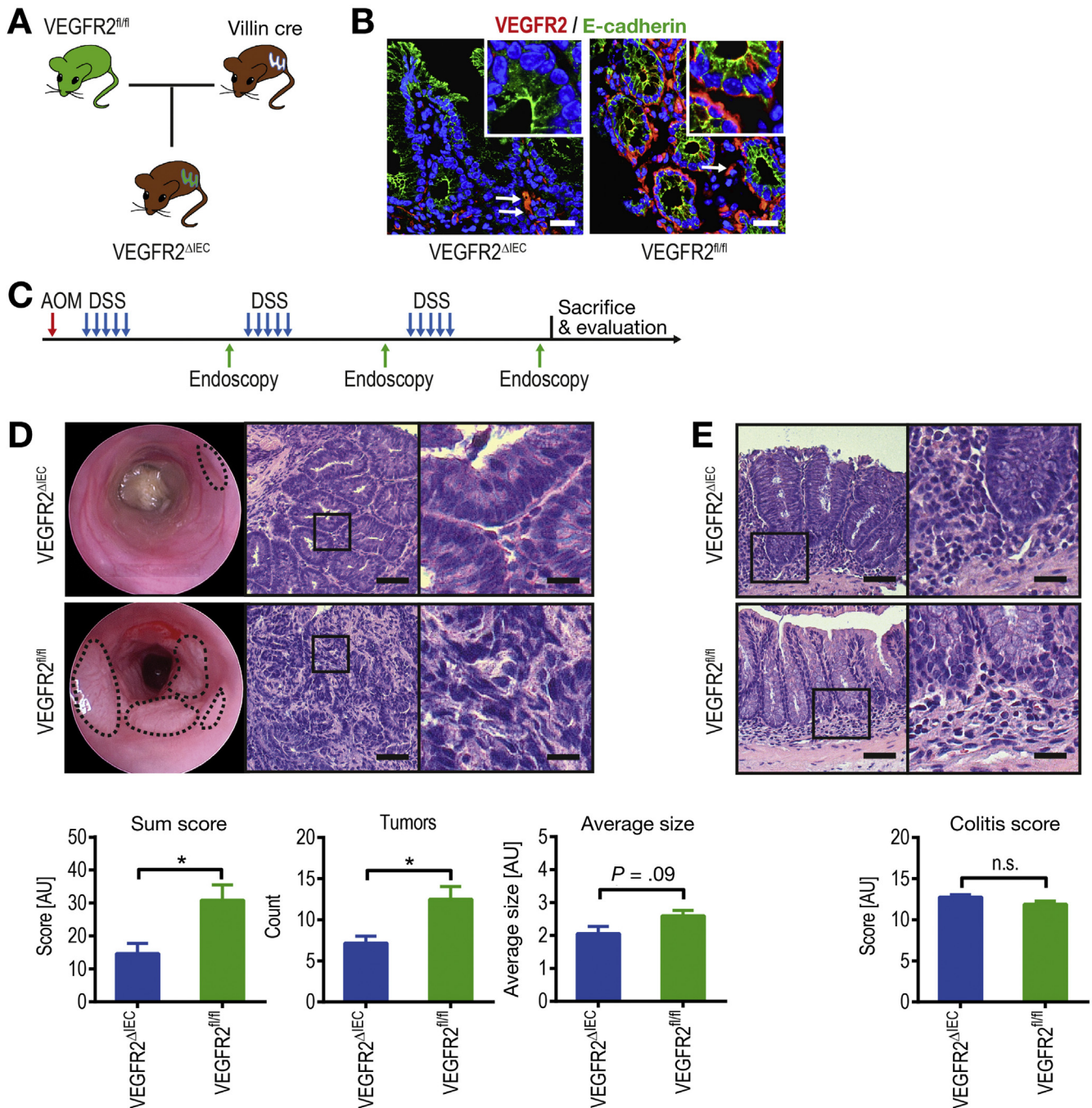
Figure 1. Loss of VEGFR2 in intestinal epithelial cells protects against tumor development in CAC. (*A*) Generation of VEGFR2$^{\Delta IEC}$ mice. (*B*) Double-staining for VEGFR2 and E-cadherin (blood vessel also labeled, *arrow*) (n = 2 mice; scale bars = 20 μm). (*C*) AOM+DSS model of colitis-associated colorectal cancer. (*D*) Endoscopy and histopathology using H&E staining of VEGFR2$^{\Delta IEC}$ and control mice. *Dashed line* surrounds visible tumors. Tumor burden (sum score), tumor count, and mean tumor size of both groups were calculated (*bar graphs*) and compared using the established endoscopic scoring system (n $\geq$ 6 mice per group; scale bars = 50 μm and 10 μm; representative of in vivo experiments in independent duplicates). (*E*) Evaluation of chronic colitis. Representative pictures of H&E-stained sections of both groups. Colitis scoring (*bar graph*) was performed using colonoscopy (n $\geq$ 6 mice per group; scale bars = 50 μm and 20 μm; representative of in vivo experiments in independent duplicates).

between VEGFR2$^{\Delta IEC}$ and control mice were irrespective of inflammation and tumor angiogenesis.

We further examined apoptosis and proliferation as potential mechanisms influencing the tumor burden. The total number of apoptotic cells in IHC was low, and there

was no difference between VEGFR2$^{\Delta IEC}$ and control mice (Figure 2E). Consistently, Western blot analysis revealed the absence of activated caspase-3 and no differences between both groups, respectively. Next, we studied tumor cell proliferation by using Ki67 and proliferating cell nuclear
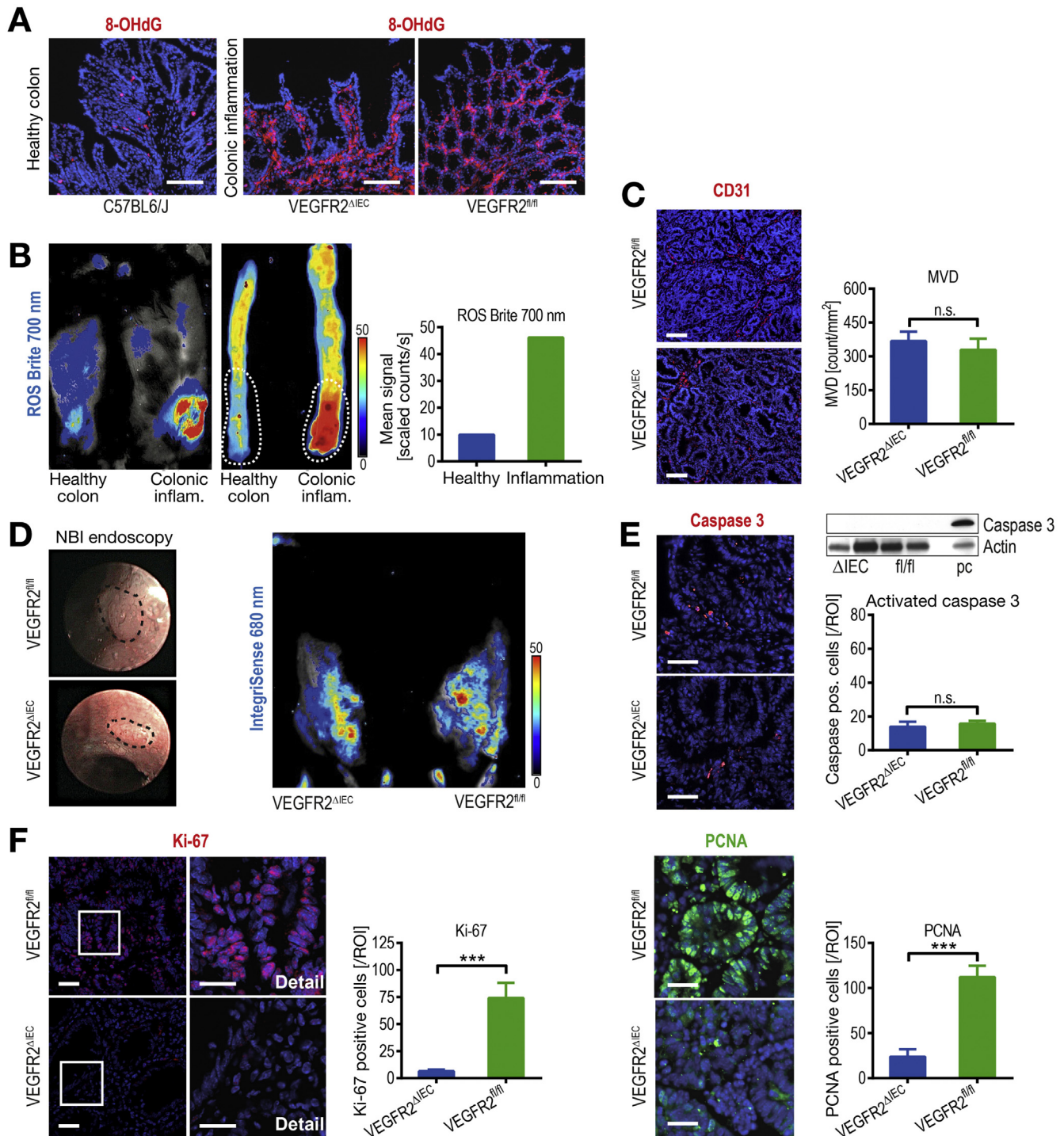
Figure 2. Molecular characterization of VEGR-2$^{\Delta IEC}$ colon and tumor tissue. (*A*) Detection of oxidative stress using 8-hydroxydesoxyguanosine (8-OHdG) staining of colonic tissue. Healthy mice, VEGFR2$^{\Delta IEC}$ mice and VEGFR2$^{fl/fl}$ mice were compared (n = 3 mice; scale bars = 100 μm). (*B*) In vivo full-body fluorescence detection of reactive oxygen species using the ROS Brite 700 nm dye. Strong signal in the distal colon is indicated (n = 3 mice). (*C*) CD31 staining detecting tumor vasculature in conditional knockout and control tumors (n ≥ 3 mice per group; scale bars = 100 μm). MVD in tumors of VEGFR2$^{\Delta IEC}$ mice and control mice was calculated and compared. (*D*) Narrow-band imaging endoscopy (NBI) and macroscopic fluorescence detection of tumor vasculature after application of a specific dye targeting the αVβ3-integrin (Integrisense; n = 3 mice). (*E*) IHC of activated caspase-3 was performed and positive cell count was used to compare both groups (n ≥ 3 mice per group; scale bars = 20 μm). Additionally, Western blot analysis of activated caspase-3 in tumor tissue of both VEGFR2$^{\Delta IEC}$ and control mice (pc, positive control). (*F*) Ki-67 and proliferating cell nuclear antigen staining with positive cell count was used to assess tumor cell proliferation in VEGFR2$^{\Delta IEC}$ and control mice (n ≥ 3 mice per group; scale bars = 50 μm and 25 μm; in vivo experiments for tissue collection for IHC analysis were performed in independent duplicates).

antigen IHC staining. Nuclear staining for Ki67 and proliferating cell nuclear antigen in epithelial tumor cells was suppressed in tumors of VEGFR2$^{\Delta IEC}$ mice compared with tumors of age-matched controls (Figure 2F), suggesting that reduction of tumor cell proliferation contributed to the significantly lower tumor development in VEGFR2$^{\Delta IEC}$ mice.

Deficient Epithelial Vascular Endothelial Growth Factor Receptor 2 Signaling Enables Premature Senescence in Colonic Tumor Cells

A low number of proliferating cells can be indicative of a tissue under growth arrest, that is, due to cellular senescence. Cellular senescence represents a prominent tumor
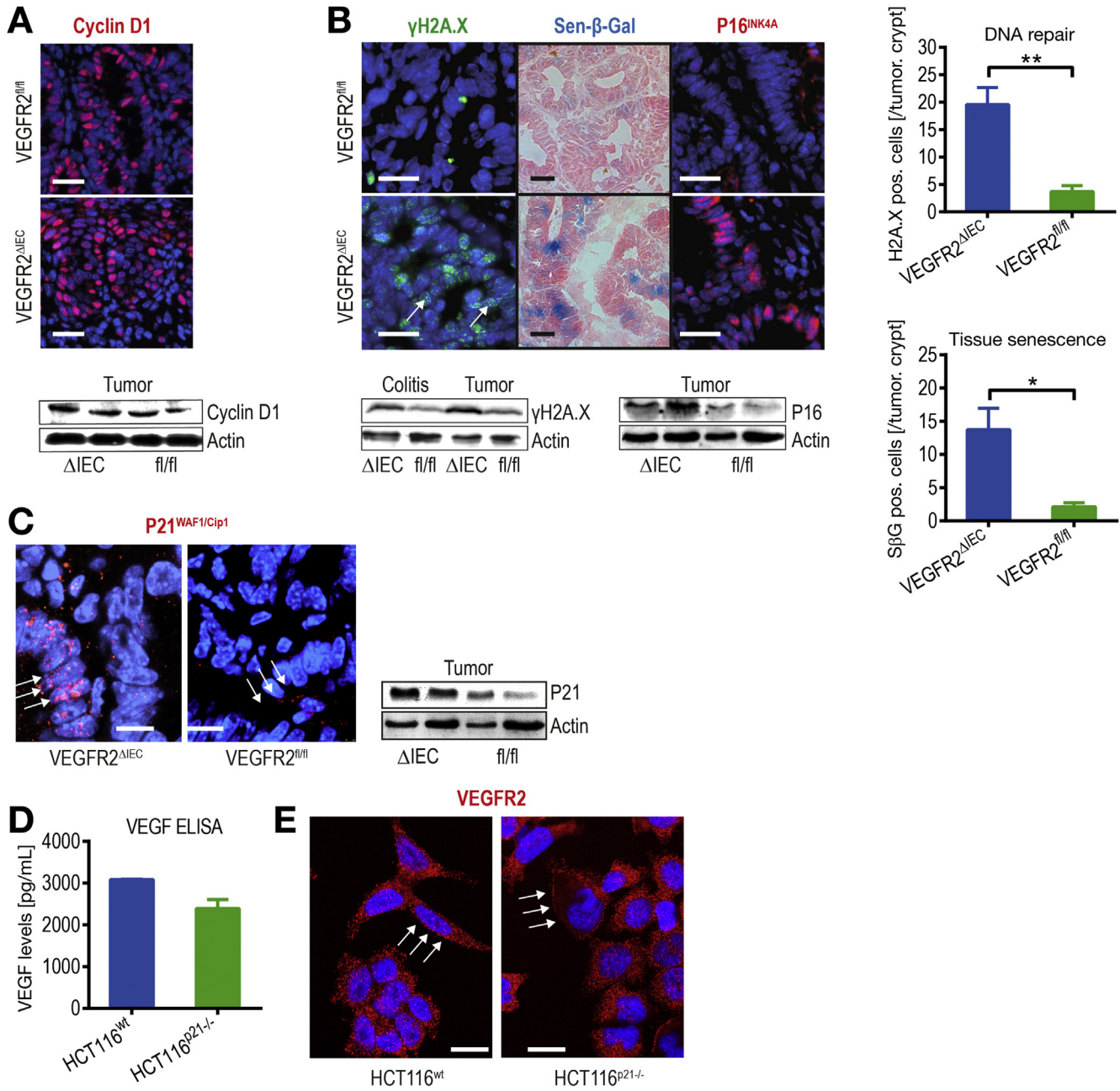
Figure 3. Deficient VEGFR2 signaling enables premature senescence in tumor cells. (A) Cyclin D1 levels were evaluated by IHC and Western blot (WB) in tumor tissue of VEGFR2$^{\Delta IEC}$ and control mice (Scale bars = 25 μm). (B) Markers for cellular senescence (γH2A.X foci [*arrows*], Sen-β-Gal, p16) were examined in tumors of VEGFR2$^{\Delta IEC}$ mice and compared with tumor tissue of control mice by IHC and WB analysis. (n ≥ 3 mice per group; scale bars = 25 μm; in vivo experiments for tissue collection for IHC analysis were performed in independent duplicates). (C) P21 was evaluated using IHC and WB in tumor tissue of VEGFR2$^{\Delta IEC}$ and control mice. *Arrows* indicate nuclear or cytoplasmatic localization of p21 (n ≥ 3 mice per group; scale bars = 10 μm). D-HCT116^{wt} and HCT116$^{p21-/-}$ colorectal carcinoma cells were examined in vitro for VEGF secretion using enzyme-linked immunosorbent assay. (E) Both cell lines express the VEGFR2 on their surface (*arrows*). Cell nuclei are counterstained with 4′,6-diamidino-2-phenylindole (*blue*) (scale bars = 10 μm).
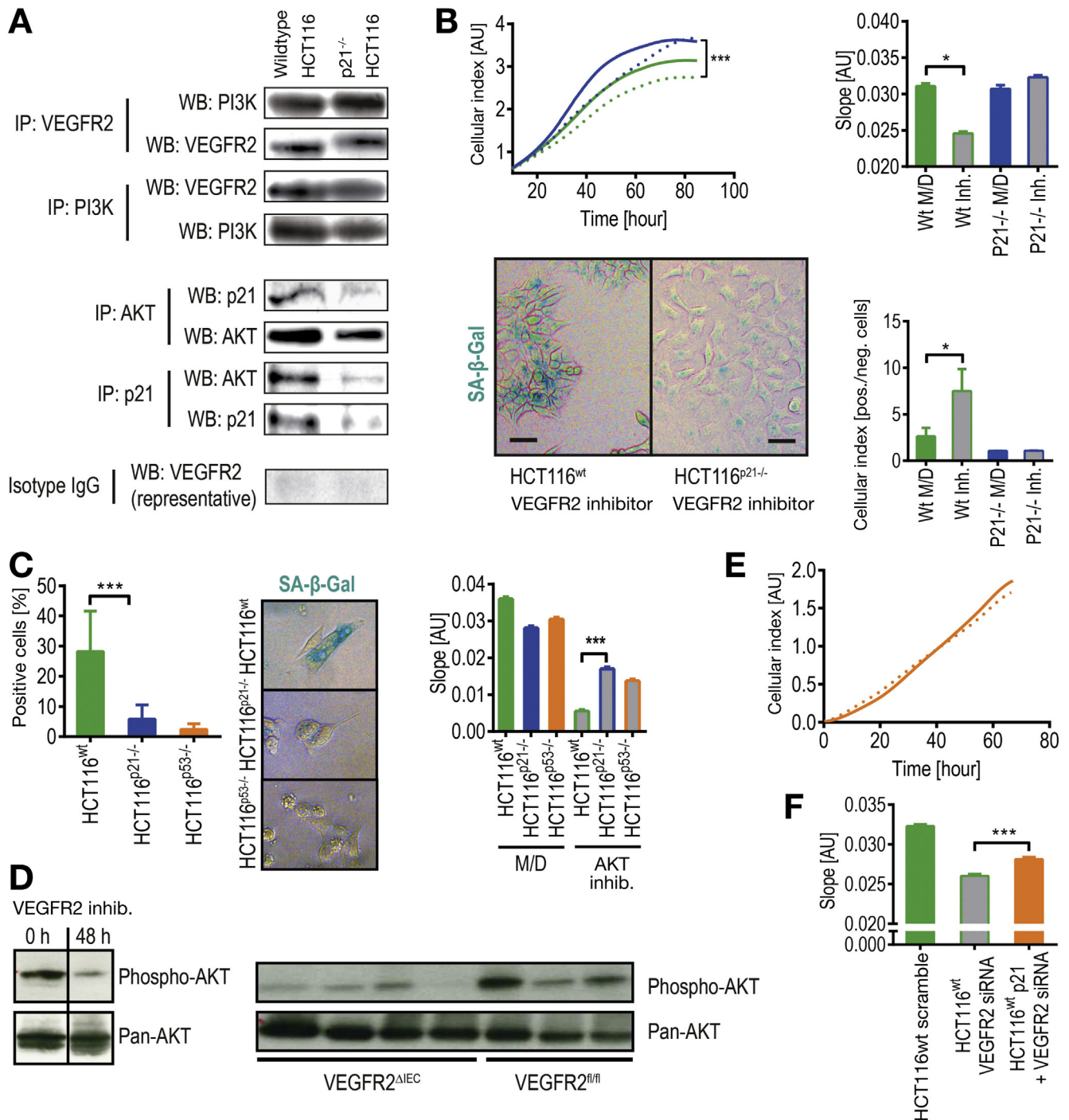
BASIC AND TRANSLATIONAL AT

Figure 4. Antiproliferative effects of VEGFR2 inhibition in tumor cells are dependent on the induction of senescence via p21 activation. (*A*) Co-immunoprecipitation shows a cascade involving the VEGFR2, PI3K, AKT, and p21 in HCT116^{wt} cells. Isotype controls are shown. (*B*) In vitro dynamic growth monitoring with the xCELLigence system of HCT116^{wt} and HCT116$^{p21-/-}$ cells after 500 nM VEGFR2 inhibition with AZD-2171 (HCT116^{wt} control: *solid green*; HCT116^{wt} with inhibitor: *dashed green*; HCT116$^{p21-/-}$ control: *solid blue*; HCT116$^{p21-/-}$ with inhibitor: *dashed blue*). Growth curves and their slopes were compared (*upper panel*). Quantification of cellular senescence as detected by Sen-β-Gal and positive cell count (*lower panel*). M/D denotes medium/dimethyl sulfoxide. (*C*) Quantification of cellular senescence by Sen-β-Gal−positive cell count in HCT116^{wt}, HCT116$^{p21-/-}$, and HCT116$^{p53-/-}$ cells after 15 μM AKT inhibition with sc-203809 (*left panel*). Also, slopes of in vitro dynamic growth monitoring of these cells were compared (*right panel*). (*D*) Western blot (WB) of phospho-AKT and pan-AKT before (0 hours) and after (48 hours) VEGFR2 inhibition (*left panel*). WB of phospho-AKT and pan-AKT in tumors of VEGFR2$^{\Delta IEC}$ and control mice (*right panel*, n = 4 vs 3). (*E*) HCT116$^{p53-/-}$ cells after inhibition with VEGFR2 (*solid orange*) shows no growth inhibition as compared with control (*dashed orange*). (*F*) Slopes of xCELLigence growth curves of HCT116^{wt} cells after treatment with VEGFR2 small interfering RNA (siRNA) alone or in combination with p21 siRNA. Scale bars = 25 μm; all in vitro growth measurements were performed in independent duplicates with matching results.
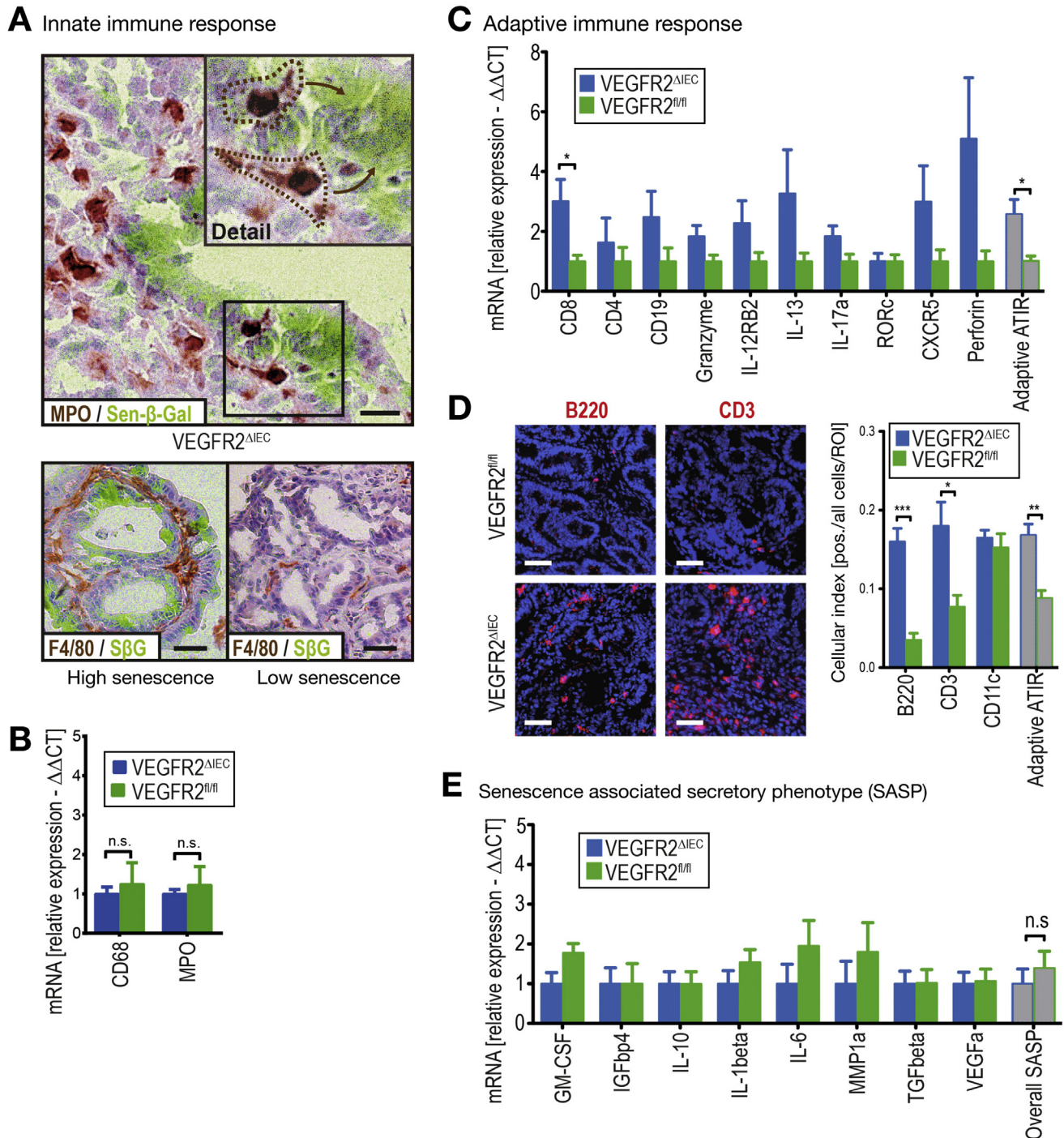
Figure 5. Innate and adaptive immune response and the senescence-associated secretory phenotype (SASP) in senescent tumors of VEGFR2$^{\Delta IEC}$ mice. (A) Myeloperoxidase (MPO)-positive cells (*dashed outline*) of the innate immune response co-localized in areas with cells positive for Sen-β-Gal staining. Sen-β-Gal is shown in false colors (*yellow-green*). F4/80-positive myeloid cells cluster near senescent cells, but are absent in tumor areas with low number of tissue senescence. All double stainings were performed in tumor tissue of VEGFR2$^{\Delta IEC}$ mice (n = 3 mice; scale bars = 20 μm and 50 μm). (B) qPCR of different markers of the innate immune response was used in whole tumor tissue (n $\geq$ 5 per group). (C) qPCR of different markers for adaptive ATIR was used in tumor tissue of VEGFR2$^{\Delta IEC}$ and control mice (n $\geq$ 4 mice per group). (D) IHC of VEGFR2$^{\Delta IEC}$ and wild-type tumor tissue was used to detect various cell types of the adaptive ATIR, such as B cells, CD3 cells, and CD11c dendritic cells (n $\geq$ 3 mice per group; scale bars = 50 μm). (E) SASP components were examined using qPCR. (n $\geq$ 4 mice per group; in vivo experiments for tissue collection were performed in independent duplicates).

suppressor mechanism that leads to permanent cell cycle arrest and can be evaluated by a combination of different markers (Supplementary Table 1). To distinguish quiescence from cellular senescence, we used Western blotting and IHC. We observed high amounts of cyclin D1 in tumors of VEGFR2$^{\Delta IEC}$ and control mice (Figure 3A). As cyclin D1 content has been shown to peak in late G1 phase during cellular senescence, and low cyclin D1 levels are found in quiescent cells in the early G0 phase,[20,21] these findings were consistent with the concept that tumors of VEGFR2$^{\Delta IEC}$ mice are in a senescent rather than a quiescent state.

We further analyzed specific markers for cellular senescence in tumors and inflamed colon tissue of knockout and control animals. Altered tissue of VEGFR2$^{\Delta IEC}$ mice revealed stronger expression of γH2A.X when compared with control mice using Western and IHC analysis (Figure 3B). Additional markers of cellular senescence were significantly higher expressed in VEGFR2$^{\Delta IEC}$ tumors when compared with tumors from VEGFR2$^{fl/fl}$ animals. Specifically, Sen-β-Gal[22] and the cyclin-dependent kinase inhibitor p16^{INK4A} (Figure 3B),[23] were significantly up-regulated in tumors of VEGFR2$^{\Delta IEC}$ mice compared with controls (Figure 3B).

Antiproliferative Effects of Vascular Endothelial Growth Factor Receptor 2 Inhibition in Tumor Cells Are Dependent on the Induction of Senescence via p21 Modification

Up-regulation of nuclear p21 is critical for the induction and maintenance of cellular senescence in various cells.[24] We observed a significant difference in p21 protein expression in tumors of VEGFR2-deficient mice compared with control mice, as assessed by Western blotting and IHC (Figure 3C). In addition, not only the overall concentration of p21 was distinctively up-regulated in tumors of VEGFR2$^{\Delta IEC}$ mice, but also a predominant nuclear staining pattern could be observed (Figure 3C). P21 is inactivated in the cytoplasm by the protein kinase AKT via post-translational mechanisms.[25] Interestingly, AKT might be mechanistically connected to VEGFR2 signaling via the PI3K.[26,27] To analyze this hypothesis, we used the human CRC cell line HCT116 with wild-type p21 or p21-deficiency (HCT116$^{p21-/-}$ cells). qPCR confirmed p21 deficiency in HCT116$^{p21-/-}$ cells (Supplementary Figure 1C). Additionally, VEGF production by these cells was examined using enzyme-linked immunosorbent assay demonstrating paracrine/autocrine VEGF production by both cell lines (Figure 3D). IHC studies revealed marked VEGFR2 expression in either HCT116^{wt} or HCT116$^{p21-/-}$ cells (Figure 3E).

Using co-immunoprecipitation, we were able to show an interaction of VEGFR2 and PI3K as well as AKT and p21, consistent with the idea of a functional connection of these molecules (Figure 4A). PI3K affects AKT via second messenger and does not require direct molecule−molecule interaction.[28] To further investigate the cascade, we used dynamic real-time growth monitoring of cell cultures (xCELLigence; Roche, Basel, Switzerland) after inhibition of VEGFR2 in HCT116^{wt} and HCT116$^{p21-/-}$ cells. VEGFR2 inhibition was able to induce growth arrest in HCT116^{wt} cells, and p21-deficient HCT116 cells showed less affected growth (Figure 4B). VEGFR2 inhibition resulted in cellular senescence in HCT116^{wt} cells, while HCT116$^{p21-/-}$ cells showed significantly less Sen-β-Gal−positive cells (Figure 4B). This suggests that the VEGFR2 signaling pathway controls cellular senescence in CRC cells. This was further confirmed in RKO cells after p21 inhibition using a small interfering RNA knockdown strategy for p21 (Supplementary Figure 2A and B). Interestingly, the effect was not as intense as in HCT116 cells. Although our data suggest that in the in vivo system, inflammation functions as a trigger to induce cellular senescence, in CRC cells, oncogene-induced senescence might serve as this stimulus in vitro.

To show an involvement of AKT in our model, a specific AKT inhibitor was used in a similar fashion as the VEGFR2 inhibitor. AKT inhibition resulted in induction of Sen-β-Gal positivity and growth inhibition in CRC cells (Figure 4C, Supplementary Figure 2C). Again, the inhibitory effect was reduced in p21-deficient and interestingly also in p53-deficient HCT116 cells. The rescue was not as pronounced as with the VEGFR2 inhibitor. Also, the levels of phosphorylated (activated) AKT decreased after VEGFR2 inhibition in CRC cells (Figure 4D). Confirming these in vitro results, we could also observe reduced levels of phospho-AKT in VEGFR2$^{\Delta IEC}$ tumors when compared with tumor tissue of control mice (Figure 4D). Similar to our results using the AKT inhibitor in HCTp53$^{-/-}$ cells, VEGFR2 inhibition had no influence on cell growth in p53-deficient HCT116 cells (Figure 4E). To verify the results achieved with the tyrosine kinase inhibitor, we also used small interfering RNA−based inhibition of VEGFR2 and p21 (Figure 4F).

Induction of Tumor Cell Senescence Is Dependent on p21 and Promotes a Functionally Relevant Anti-Tumor Immune Response

Although the induction of cellular senescence limits proliferation in aberrant cells directly, senescent cells remain within the tissue and do not immediately undergo cell death.[29] However, senescent tumor cells have been

Figure 6. The induction of tumor cell senescence promotes a functional relevant ATIR. (A) Experimental protocol. C57BL/6 mice with and without CD8$^+$ T-cell depletion and p21$^{-/-}$ mice were examined. All mice received VEGFR2 inhibitor. (B) MVD in tumor tissue was compared from p21-deficient, CD8$^+$ T-cell−depleted mice receiving VEGFR2 inhibitor and mice only receiving the drug. CD31 staining was used to identify vessels. (C) Endoscopic scores of tumor burden (sum score), tumor size, tumor count, and degree of colitis were evaluated after AOM+DSS. (D) Representative endoscopic and histopathologic images are shown. *Dashed line* surrounds visible tumors (n $\geq$ 5 mice per group; scale bars = 200 μm). (E) Sen-β-Gal staining of the 3 groups was performed and positive cells were counted (n = 2 per group; scale bars = 100 μm).

shown to be subject to enhanced immunosurveillance. To analyze this in our model, we performed double staining for F4/80 and myeloperoxidase with Sen-β-Gal in colonic tissue from mice with CAC. We could identify F4/80- and myeloperoxidase-expressing macrophages and granulocytes in tumor areas with high numbers of senescent cells (Figure 5A). We also examined whole tissue via qPCR for markers of the innate immune response, but counterintuitively could not find a significant difference. This might be due to the heterogeneity of the tissue (Figure 5B).

Apart from the innate immune system, the adaptive immune system driven by CD4+ and CD8+ T cells has been proposed to play a crucial role in anti-tumor immune response (ATIR), especially in colorectal neoplasia.[30] So we performed qPCR and IHC for markers of ATIR. VEGFR2$^{\Delta IEC}$ tumors showed a mean 2-fold increase for ATIR markers, which was statistically significant for CD8+ T cells (Figure 5C). Additionally, IHC showed a significantly increased infiltrate of B and T cells, when conditional knockout and control tumor tissues were compared (Figure 5D). We then looked at different components of the senescence-associated secretory phenotype, which plays an important role in the inflammatory micromilieu.[31,32] However, qPCR did not demonstrate differences in senescence-associated secretory phenotype between control and VEGFR2$^{\Delta IEC}$ tissues in our model (Figure 5E).

To evaluate the interaction of the adaptive immune system and senescent tumor cells on a functional level, we performed the AOM+DSS model in wild-type and p21$^{-/-}$ mice in the presence of a VEGFR2 inhibitor (Figure 6A). Optimal dosage and potency of the VEGFR2 inhibitor to inhibit tumor growth and induce cellular senescence were confirmed in an initial set of experiments (Supplementary Figure 3A). In addition, to directly study the functional role of CD8+ T cells during ATIR, antibody-mediated CD8+ depletion was performed in one group (Supplementary Figure 3B). To exclude an effect of VEGFR2 inhibition on tumor vasculature, we performed MVD calculation. There was no difference in MVD measurement in tumors of mice treated with VEGFR2 inhibitor only when compared with tumors of p21-deficient mice or CD8+ T-cell–depleted mice also treated with the drug (Figure 6B).

Endoscopy revealed that mice with either impaired induction of cellular senescence or impaired ATIR showed a significantly higher tumor count, as well as a significantly higher tumor burden, similar to untreated control animals, as compared with mice receiving VEGFR2 inhibitor only (Figure 6C and D, and Supplementary Figure 4). Using Sen-β-Gal staining, we could detect significantly more senescent tumor cells in C57BL/6 mice when compared with p21$^{-/-}$ mice both treated with the VEGFR2 inhibitor, whereas AOM+DSS induced tumors in wildtype mice without VEGFR2 inhibitor treatment did not show Sen-β-Gal positivity (Figure 6E and Supplementary Figure 3C). In line with our experiments, p21$^{-/-}$ mice without VEGFR2 inhibition did not show any differences regarding tumor growth in comparison with untreated wild-type mice (Supplementary Figure 5A and B).

The Possibility of Inducing Senescence in Tumor Cells Upon Anti−Vascular Endothelial Growth Factor Treatment Correlates With the Prognosis of Colorectal Cancer Patients

To address whether the induction or maintenance of cellular senescence is clinically relevant in CRC patients, tissue samples of CRCs before and after anti-VEGF treatment were evaluated. In these studies, IHC for p21 was used to assess overall expression as well as subcellular localization in a group of cancer patients (Supplementary Table 2). Tumor tissue of patients before and after therapeutic targeting of the VEGF/VEGFR2 axis showed either a predominantly cytoplasmatic or nuclear expression of p21 (Figure 7A). Cell count was used to calculate the difference of senescence induction, represented by a shift from cytoplasmatic to nuclear p21 (ΔSenescence). Whenever an increase in the nuclear-to-cytoplasmic p21 ratio could be observed upon bevacizumab therapy, patients were grouped into ΔSenescence^{Hi}, otherwise they fell into ΔSenescence^{Lo} (Supplementary Figure 6A−D). Patients with a strong induction of cellular senescence (ΔSenescence^{Hi}) showed a significantly better response to bevacizumab treatment resulting in a significantly longer progression-free survival when compared with ΔSenescence^{Lo} patients (Figure 7B). Overall survival showed a beneficiary trend in the ΔSenescence^{Hi} group, which did not reach statistical significance. In addition to the subcellular localization, signal intensity was evaluated using image analysis. Patients on a bevacizumab regimen without tumor progression (progression-free) showed significantly stronger signal intensity for p21 when compared with patients with progressive disease receiving this drug (Figure 7C). We further analyzed whether immunosurveillance of senescent cells by CD8+ T cells could play a role in patients receiving bevacizumab-based treatment (Figure 7D). Here we could show that progression-free survival significantly correlated with the induction of CD8+ T-cell infiltration. We exemplarily investigated a potential role of AKT inhibition upon targeting the VEGF/VEGFR2 axis and could find decreased levels of phospho-AKT after bevacizumab treatment (Supplementary Figure 7A) in example patients of the ΔSenescence^{Hi} group. We also examined p53 status by routine pathologic IHC analysis, but could not detect any statistically significant correlation with the induction of cellular senescence or survival parameters (Supplementary Figure 7B−D).

Discussion

During recent years, inhibition of VEGF signaling has become a cornerstone of clinical therapy in various types of cancer, including CRC.[5,33] Notwithstanding the benefit most patients gain from anti-VEGF therapeutics, it is still unknown why some patients develop resistance or do not respond to anti-VEGF treatment at all.[34] Although the pro-angiogenic effects of VEGF have been studied extensively, only recent data propose VEGF as an auto-/paracrine growth factor for tumor cells.[8,9]

Here we show for the first time that VEGFR2 signaling in epithelial cells is essential for tumor growth in a model of CAC using conditional knockout mice. In these experiments,
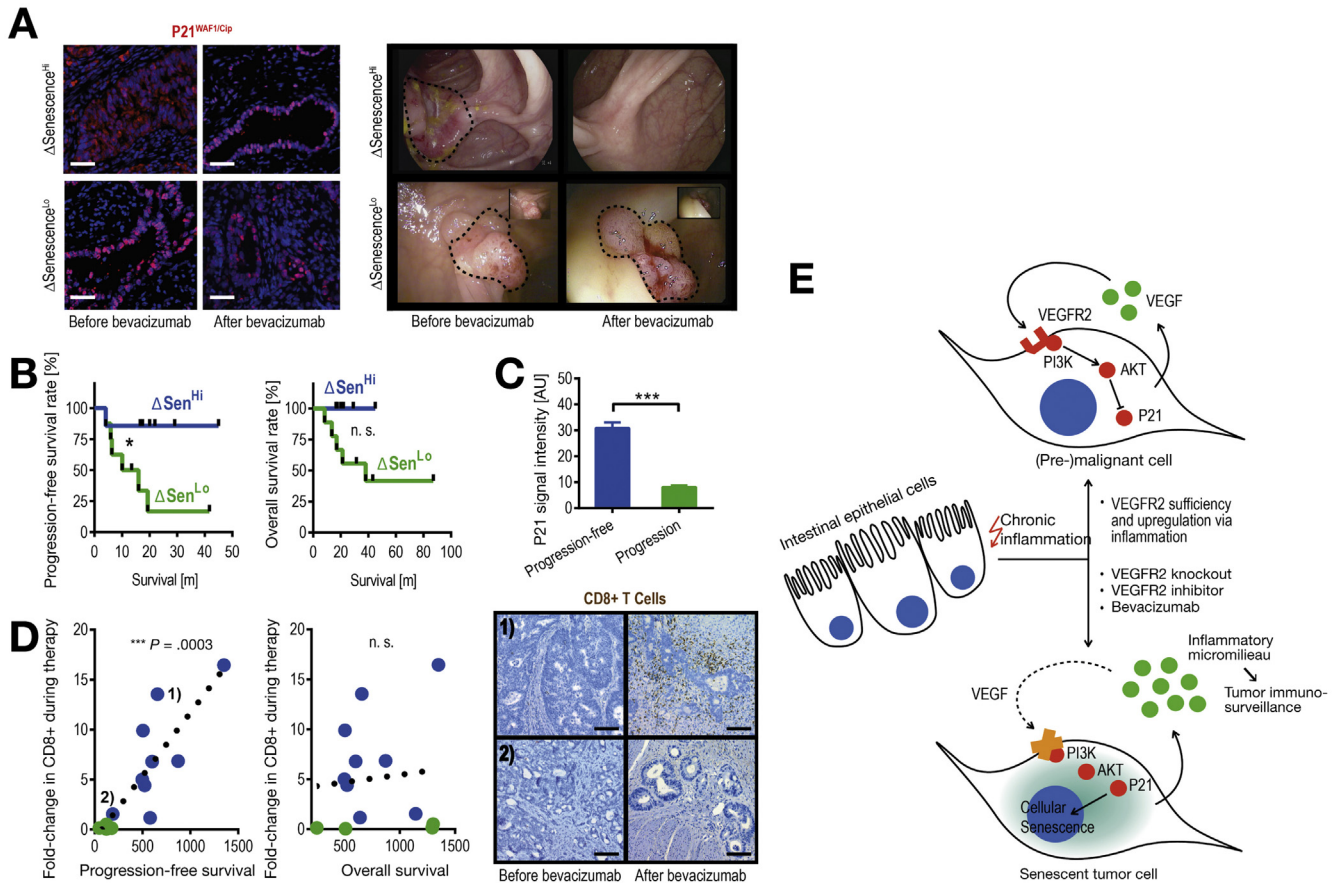
Figure 7. The possibility of inducing senescence in tumor cells upon anti-VEGF treatment correlates with the prognosis of CRC patients. (*A*) IHC staining for p21 in tumor samples of CRC patients before and after receiving bevacizumab therapy. Nuclear-to-cytoplasmatic ratio was used to group patients into ΔSenescence^{Hi} (ΔSen^{Hi}; >10% shift from cytoplasmatic to nuclear p21) and ΔSenescence^{Lo} (ΔSen^{Lo}; <10% shift from cytoplasmatic to nuclear p21 or shift from nuclear to cytoplasmatic p21). Endoscopic images of representative patients of both groups before and after bevacizumab treatment. (*B*) Progression-free and overall survival of ΔSen^{Hi} and ΔSen^{Lo} patients. (*C*) Signal intensity of p21 staining in tumor tissue of bevacizumab-treated patients. (n = 15 patients/30 samples/image analysis of 2−5 representative images per sample/; scale bars = 50 μm). (*D*) IHC for CD8$^+$ T cells was performed before and after therapy and the fold-induction (value >1) or reduction (value 0−1) was calculated and correlated to progression-free and overall survival. Representative images of 2 patients indicated in the X/Y graph are shown (n = 13 patients/26 samples/2−5 images per specimen; scale bars = 150 μm). (*E*) Model of VEGFR2-associated regulation of cellular senescence in colorectal neoplasia. Upon inflammatory stimulus, the VEGFR2 is up-regulated in intestinal epithelial cells, which leads to premalignancy. This leads to activation of the PI3K/AKT pathway, which leads to p21 inactivation in the cytoplasm. In a VEGFR2-deficient setting, VEGF cannot fulfill its senescence inhibitory functions and senescence is induced upon oxidative stress of chronic colitis.

deletion of VEGFR2 in IECs protected against inflammatory carcinogenesis, interestingly, these mice showed normal intestinal development. This can be explained by the observation that VEGFR2 is not expressed in relevant amounts by normal IECs, but gets up-regulated during inflammation or in tumor cells. In accordance with this observation, the up-regulation of VEGFR2 in dysplastic tumor cells has also been shown for other types of cancer, such as ovarian cancer.[35]

We have previously shown that VEGFR2 activation in tumor cells induces proliferation and is dependent on the activation of downstream pathways, such as signal transducer and activator of transcription 3.[36] In this study, we could also see increased proliferation in control mice in comparison with VEGFR2$^{\Delta IEC}$ mice, supporting previous

data. Interestingly, the lack of VEGFR2 signaling in tumor cells was accompanied by up-regulation of various markers for cellular senescence.

Several studies propose activation of cellular senescence during inflammation and early steps of tumor development through stress-sensing signaling pathways.[37] In this context, cellular senescence acts as a gatekeeper that induces cell cycle arrest and prevents damaged cells from further transformation and even metastasis.[38,39] For further progression, tumor cells need to bypass cellular senescence, for example, through mutations of tumor suppressor pathways that are involved in senescence activation and maintenance.[23]

In our model, cell-specific VEGFR2 deficiency was associated with cellular senescence and, therefore,

suggests that intact VEGFR2 signaling in tumor cells is a key factor for cells to actively bypass the protective effects of cellular senescence. VEGFR2 signaling has previously been suggested to "inactivate" senescence in vascular endothelial cells.[40] However, this mechanism seems to be even more relevant for tumor cells, where it has not yet been reported.

In addition, VEGF-mediated bypass of cellular senescence was dependent on post-transcriptional inactivation of p21. Similar to a study by Zhou et al on HER-2/neu signaling in breast cancer cells, VEGFR2-dependent regulation of cellular senescence was mediated through the PI3K/AKT signaling pathway.[25,41] Accordingly, systemic VEGFR2 inhibition was only effective to suppress colorectal tumor development in wild-type, but not p21-deficient mice, and, therefore, the protective effects of VEGFR2 signaling were critically dependent on p21 activation in our study.

Importantly, the induction of cellular senescence in tumor cells of VEGFR2$^{\Delta IEC}$ mice was accompanied by increased infiltration of tumor tissue with adaptive immune cells in our experiments. An increased adaptive immune response to senescent tumor cells has been shown for other tumor types. For instance, in a study by Xue et al, the induction of senescence in a murine model of hepatocellular cancer through p53 reactivation in previously p53-deficient tumor cells triggers an innate immune response that contributes to tumor regression.[29] In our study, the immune response was functionally dependent on CD8$^+$ cytotoxic T cells. This can be explained by differences in the immune response among individual types of cancer, as CD8$^+$ T cells have been shown to be a central component of anti-tumor immunity in sporadic colorectal cancer.[30,42] Paralleling these preclinical results, we could show whether an anti-VEGF regimen is proficient to induce cellular senescence, then this is accompanied by a significantly higher progression-free survival in a cohort of CRC patients.

Taken together, the results presented here propose a completely new mechanism of VEGF/VEGFR2 signaling in colorectal cancer involving the bypass of cellular senescence through VEGFR2-dependent p21 inactivation in cancer cells. As systemic VEGFR2 inhibition enabled cellular senescence in tumor cells, followed by a functional relevant ATIR, this effect might also be involved in the therapeutic effects of anti-VEGF treatment of human CRC (Figure 7E).

Supplementary Material

References

1. Pitot HC. The molecular biology of carcinogenesis. Cancer 1993;72:962–970.

2. Grivennikov SI, Greten FR, Karin M. Immunity, inflammation, and cancer. Cell 2010;140:883–899.

3. Ferrara N, Gerber H-P, LeCouter J. The biology of VEGF and its receptors. Nat Med 2003;9:669–676.

4. Kerbel RS. Tumor angiogenesis. N Engl J Med 2008;358:2039–2049.

5. Hurwitz H, Fehrenbacher L, Novotny W, et al. Bevacizumab plus irinotecan, fluorouracil, and leucovorin for metastatic colorectal cancer. N Engl J Med 2004;350:2335–2342.

6. Lee T-H, Seng S, Sekine M, et al. Vascular endothelial growth factor mediates intracrine survival in human breast carcinoma cells through internally expressed VEGFR1/FLT1. PLoS Med 2007;4:e186.

7. Beck B, Driessens G, Goossens S, et al. A vascular niche and a VEGF-Nrp1 loop regulate the initiation and stemness of skin tumours. Nature 2011;478:399–403.

8. Hamerlik P, Lathia JD, Rasmussen R, et al. Autocrine VEGF-VEGFR2-Neuropilin-1 signaling promotes glioma stem-like cell viability and tumor growth. J Exp Med 2012;209:507–520.

9. Waldner MJ, Wirtz S, Jefremow A, et al. VEGF receptor signaling links inflammation and tumorigenesis in colitis-associated cancer. J Exp Med 2010;207:2855–2868.

10. Deng C, Zhang P, Harper JW, et al. Mice lacking p21CIP1/WAF1 undergo normal development, but are defective in G1 checkpoint control. Cell 1995;82:675–684.

11. Haigh JJ, Morelli PI, Gerhardt H, et al. Cortical and retinal defects caused by dosage-dependent reductions in VEGF-A paracrine signaling. Dev Biol 2003;262:225–241.

12. Nakayama M, Nakayama A, van Lessen M, et al. Spatial regulation of VEGF receptor endocytosis in angiogenesis. Nat Cell Biol 2013;15:249–260.

13. el Marjou F, Janssen K-P, Chang BH-J, et al. Tissue-specific and inducible Cre-mediated recombination in the gut epithelium. Genesis 2004;39:186–193.

14. Becker C, Fantini MC, Schramm C, et al. TGF-beta suppresses tumor progression in colon cancer by inhibition of IL-6 trans-signaling. Immunity 2004;21:491–501.

15. Waldner MJ, Wirtz S, Neufert C, et al. Confocal laser endomicroscopy and narrow-band imaging-aided endoscopy for in vivo imaging of colitis and colon cancer in mice. Nat Protoc 2011;6:1471–1481.

16. Becker C, Fantini MC, Wirtz S, et al. In vivo imaging of colitis and colon cancer development in mice using high resolution chromoendoscopy. Gut 2005;54:950–954.

17. Neufert C, Becker C, Neurath MF. An inducible mouse model of colon carcinogenesis for the analysis of sporadic and inflammation-driven tumor progression. Nat Protoc 2007;2:1998–2004.

18. Neurath MF, Wittkopf N, Wlodarski A, et al. Assessment of tumor development and wound healing using endoscopic techniques in mice. Gastroenterology 2010;139:1837–1843.e1.

19. Scaldaferri F, Vetrano S, Sans M, et al. VEGF-A links angiogenesis and inflammation in inflammatory bowel disease pathogenesis. Gastroenterology 2009;136:

585–595.e5.

20. Blagosklonny MV. Cell cycle arrest is not senescence. Aging 2011;3:94–101.

21. Pajalunga D, Mazzola A, Salzano AM, et al. Critical requirement for cell cycle inhibitors in sustaining non-proliferative states. J Cell Biol 2007;176:807–818.

22. Dimri GP, Lee X, Basile G, et al. A biomarker that identifies senescent human cells in culture and in aging skin in vivo. Proc Natl Acad Sci U S A 1995;92:9363–9367.

23. Serrano M, Lin AW, McCurrach ME, et al. Oncogenic ras provokes premature cell senescence associated with accumulation of p53 and p16INK4a. Cell 1997; 88:593–602.

24. Fragkos M, Jurvansuu J, Beard P. H2AX is required for cell cycle arrest via the p53/p21 pathway. Mol Cell Biol 2009;29:2828–2840.

25. Zhou BP, Liao Y, Xia W, et al. Cytoplasmic localization of p21Cip1/WAF1 by Akt-induced phosphorylation in HER-2/neu-overexpressing cells. Nat Cell Biol 2001;3:245–252.

26. Laramée M, Chabot C, Cloutier M, et al. The scaffolding adapter gab1 mediates vascular endothelial growth factor signaling and is required for endothelial cell migration and capillary formation. J Biol Chem 2007;282:7758–7769.

27. Dance M, Montagner A, Yart A, et al. The adaptor protein Gab1 couples the stimulation of vascular endothelial growth factor receptor-2 to the activation of phosphoinositide 3-kinase. J Biol Chem 2006;281:23285–23295.

28. Luo J, Manning B, Cantley L. Targeting the PI3K-Akt pathway in human cancer—rationale and promise. Cancer Cell 2003;4:257–262.

29. **Xue W, Zender L**, Miething C, et al. Senescence and tumour clearance is triggered by p53 restoration in murine liver carcinomas. Nature 2007;445:656–660.

30. Galon J, Costes A, Sanchez-Cabo F, et al. Type, density, and location of immune cells within human colorectal tumors predict clinical outcome. Science 2006; 313:1960–1964.

31. Coppé J-P, Desprez P-Y, Krtolica A, et al. The senescence-associated secretory phenotype: the dark side of tumor suppression. Annu Rev Pathol 2010;5:99–118.

32. Kuilman T, Peeper DS. Senescence-messaging secretome: SMS-ing cellular stress. Nat Rev Cancer 2009; 9:81–94.

33. Miller K, Wang M, Gralow J, et al. Paclitaxel plus bevacizumab versus paclitaxel alone for metastatic breast cancer. N Engl J Med 2007;357:2666–2676.

34. Longo R, Gasparini G. Challenges for patient selection with VEGF inhibitors. Cancer Chemother Pharmacol 2007;60:151–170.

35. Spannuth WA, Nick AM, Jennings NB, et al. Functional significance of VEGFR-2 on ovarian cancer cells. Int J Cancer 2009;124:1045–1053.

36. Schaefer LK, Ren Z, Fuller GN, et al. Constitutive activation of Stat3alpha in brain tumors: localization to tumor endothelial cells and activation by the endothelial tyrosine kinase receptor (VEGFR-2). Oncogene 2002; 21:2058–2065.

37. Collado M, Serrano M. Senescence in tumours: evidence from mice and humans. Nat Rev Cancer 2010;10:51–57.

38. Schmitt C, Fridman J, Yang M, et al. A senescence program controlled by p53 and p16 INK4a contributes to the outcome of cancer therapy. Cell 2002;109:335–346.

39. Ansieau S, Bastid J, Doreau A, et al. Induction of EMT by twist proteins as a collateral effect of tumor-promoting inactivation of premature senescence. Cancer Cell 2008;14:79–89.

40. **Bais C, van Geelen A**, Eroles P, et al. Kaposi's sarcoma associated herpesvirus G protein-coupled receptor immortalizes human endothelial cells by activation of the VEGF receptor-2/KDR. Cancer Cell 2003;3:131–143.

41. **Zhou BP, Liao Y**, Xia W, et al. HER-2/neu induces p53 ubiquitination via Akt-mediated MDM2 phosphorylation. Nat Cell Biol 2001;3:973–982.

42. Pagès F, Galon J, Dieu-Nosjean M-C, et al. Immune infiltration in human tumors: a prognostic factor that should not be ignored. Oncogene 2010;29:1093–1102.

BASIC AND TRANSLATIONAL AT

Supplementary Material

Animal Models (Continued)

Before further tissue evaluation, mice were sacrificed by cervical dislocation under isoflurane anesthesia (Abbvie, North Chicago, IL). Healthy and tumorous colonic tissue was gathered for further tissue analysis. For epithelial cell isolation, the colon was incubated at 37°C in HBSS containing 2 mM EDTA, 1 mM ethylene glycol-bis(β-aminoethyl ether)-*N,N,N′,N′*-tetraacetic acid, and 1% fetal calf serum for 15 minutes.

Endoscopy, Narrow-Band Imaging, Full-Body Fluorescence Imaging (Continued)

The MAESTRO full-body fluorescence scanning system was used for multispectral fluorescence analysis in vivo. Fluorescence imaging of integrin $\alpha V\beta 3$ was performed 1 day after intravenous injection of fluorescence imaging agent IntegriSense (100 μL per animal; VisEn Medical, Bedford, MA). Detection of reactive oxygen species was performed using the ROS Brite 700 nm dye according to the manufacturer's guidelines (AAT Bioquest). Final concentration was 10 μg/g body weight administered intravenously, 20 minutes before examination. For all the procedures, animals were under deep sedation using isoflurane as inhalative anesthetic.

Administration of Vascular Endothelial Growth Factor Receptor 2 Inhibitor, CD8^{+} Depletion Antibody (Continued)

Animals were then equally assigned to the groups to ensure matching tumor scores before the administration of each compound. VEGFR2 inhibitor (CHIR-258; Selleck Chemicals, Boston, MA) was administered orally via feeding tube every 48 hours in a concentration of approximately 15 μg/g body weight for a duration of 4 weeks. CD8^{+} T-cell depletion was achieved via anti−CD8-antibody treatment (BioXcell BE0004-1, mCD8a, Clone 53-6.72). Ten micrograms per gram body weight were administered intraperitoneally twice a week.

Immunohistochemistry

Cryosections were made of frozen tissue specimens, fixed with 4% paraformaldehyde, and sequentially incubated with methanol, avidin/biotin (Vector Laboratories, Burlingame, CA), protein-blocking reagent (Dako, Carpinteria, CA) and mouse-on-mouse IgG blocking reagent if necessary. Primary antibodies specific for p21, E-cadherin, VEGFR2, p16, cyclin D1, myeloperoxidase, F4/80, CD3, Ki67, 8-hydroxydesoxyguanosine, B220, proliferating cell nuclear antigen, CD8 were dissolved in Tris-buffered saline and Tween 20/0.5% bovine serum albumin and incubated overnight at 4°C. For negative controls, the primary antibody was omitted. Furthermore, anti-VEGFR2, p16 and p21 antibodies from different manufacturers were tested to ensure specificity (Cell Signaling Technology, Abcam, Santa Cruz Biotechnology). Subsequently, slides were incubated with biotinylated secondary antibodies and streptavidin-horseradish peroxidase and stained with Tyramide (Cy3 and fluorescein isothiocyanate) or 3,3′-diaminobenzidine tetra hydrochloride according to the manufacturer's protocol (PerkinElmer, Waltham, MA). Nuclei were counterstained with 4′,6-diamidino-2-phenylindole (DAPI; Vector Laboratories). Next, brightfield-, fluorescence- (Leica), or confocal microscopy (SP5; Leica, Buffalo Grove, IL) was performed. Quantification of IHC staining was performed with ImageJ software (National Institutes of Health, Bethesda, MD) automatically or via cell counting by hand. Positive cells were counted per longitudinal crypt, tumorous crypt, or region of interest, respectively, usually 2−10 crypts or regions of interest of a representative tumor were counted per mouse. If not indicated otherwise, n ≥ 3 mice per group were analyzed. Whenever applicable (ie, immune cell infiltration), positive cells were normalized to total number of cells as detected by DAPI staining. Nuclear staining was defined as DAPI and fluorophore colocalization, cytoplasmatic staining was present when a DAPI-positive nucleus was surrounded by fluorophore-positive cytoplasm. Signal intensity was evaluated by calculating mean red-/green-scale values in tumor specific regions of interest. For better visualization of representative images, brightness and contrast might have been adjusted, while always making sure all changes applied to the whole image. For further detail see Supplementary Figure 5.

Senescence-Associated B Galactosidase Assay (Continued)

Live cells were cultured in 6-well plates and treated with VEGFR2 inhibitors as described here. After washing with phosphate-buffered saline, cells were fixed with fixative solution according to the manufacturer's protocol. Incubation with pH-adjusted Sen-β-Gal staining was carried out overnight at 37°C. Tissue sections and live cells were analyzed using brightfield microscopy. Usually, at least 3 wells were analyzed cell type or treatment.

Western Blot Analysis and Co-Immunoprecipitation

Western blotting was routinely performed as described previously. Specific antibodies against VEGFR2, cleaved caspase-3, cyclin D1, p21, γH2A.X, p16, PI3K, and AKT were used. Detection of specific bands was performed with the ECL Western blotting analysis system (PerkinElmer). For activated caspase-3 detection cells with deletion of apoptosis inhibitor served as positive control. Co-immunoprecipitation was performed using the Miltenyi MultiMACS Magnetic Separator System according to the manufacturer's protocol (Miltenyi Biotec, Bergisch Gladbach, Germany). In short, 500-μg protein lysate, isolated from 2×10^6 tumor cells were incubated with protein G−coupled magnetic beads (monoclonal antibodies) or protein A/G−coupled magnetic beads (polyclonal antibody) and VEGFR2, PI3K, p21, or AKT antibodies for 45 minutes. Incubation with isotype IgG served as negative control.

Isolation of precipitated protein complexes was performed using magnetic microcolumns. Precipitate was eluted with electrophoresis sample buffer and consecutive Western blotting was carried out as described here. For better visualization of representative blots, brightness and contrast might have been adjusted, while always making sure all changes applied to the whole image.

In Vitro Experiments

Human CRC cells HCT 116 and p21- or p53-deficient HCT $116^{p21-/-}$ and HCT $116^{p53-/-}$ cells, as well as RKO cells have been described previously.[1–3] Cells were cultivated in Dulbecco's modified Eagle medium ($+10\%$ fetal calf serum, 1% glutamine, 1% streptomycin, and 1% penicillin) at 37°C and 5% CO_2. In vitro dynamic growth monitoring was performed using the xCELLigence system, as advised by the manufacturer (Roche). In short, cells were seeded in 16-well e-plates and adherent growth was established overnight. VEGFR2 inhibitor (AZD-2171; Selleck Chemicals, concentration approximately 500 nM) and AKT inhibitor (sc-203809; Santa Cruz Biotechnology; concentration approximately 15 μM) were added to normal growth medium and growth curves were recorded during a period of up to 7 days. Raw data were exported and processed (normalization, smoothening, etc) using Excel and PRISM software. Same concentrations were added to cells in 6-well plates and Sen-β-Gal staining was performed as described here. Small interfering RNA experiments were performed using FlexiTube siRNA targeting p21 and VEGFR2 (Qiagen, Valencia, CA) according to the manufacturer's protocol. Several different small interfering RNAs were tested for knockdown efficiency and scramble small interfering RNA was used as control (KDR: SI00605528, SI00605535, SI00035238, SI00035252; p21: SI00299810, SI00604898, SI00604905, SI00008547; control: SI03650325).

Quantitative Analysis of Gene Expression

Total RNA was isolated from cells and organs with RNeasy columns (Qiagen), including DNase I digestion. Complementary DNA was generated using the iScript cDNA Synthesis kit (Bio-Rad Laboratories, Hercules, CA). Quantitative real-time PCR analysis for different primers (all validated by the manufacturer) and HPRT was performed using specific QuantiTect Primer/Probe assays (Qiagen) and QuantiTect Sybr Green (Qiagen). Gene expression was calculated relative to the house-keeping gene HPRT using the $\Delta\Delta$Ct algorithm.

Patient Material

Formalin-fixed, paraffin-embedded samples of 15 patients before and after bevacizumab-based chemotherapeutic regimen were obtained from the Comprehensive Cancer Center, Erlangen-Nürnberg. This was approved by the head review board in accordance with national and international guidelines. IHC for p21 was performed as described here. Clinical data were obtained from our department's gastrointestinal oncology section.

Statistical Analysis

All preclinical data were evaluated with GraphPad Prism software, version 5.00 (GraphPad, La Jolla, CA). Clinical data were documented using IBM SPSS Statistics software, version 21 (Armonk, NY). When 2 variables were compared, 2-sided, unpaired Student t test was performed. When more than 2 groups were examined, one-way analysis of variance was used. For growth curves, curve analysis was used according to GraphPad Prism software. If not indicated otherwise, the statistical mean is presented and error bars represent SEM. P values are indicated as follows: *$P < .05$; **$P < .01$; ***$P < .001$.

Supplementary References

1. Bunz F, Dutriaux A, Lengauer C, et al. Requirement for p53 and p21 to sustain G2 arrest after DNA damage. Science 1998;282:1497–1501.
2. Waldman T, Kinzler KW, Vogelstein B. p21 is necessary for the p53-mediated G1 arrest in human cancer cells. Cancer Res 1995;55:5187–5190.
3. Boyd D, Florent G, Kim P, et al. Determination of the levels of urokinase and its receptor in human colon carcinoma cell lines. Cancer Res 1988;48:3112–3116.

Author names in bold designate shared co-first authorship.

Supplementary Table 1. Table of Various Marker Sets

Markers		Proliferation	Quiescence	Senescence	VEGFR2$^{\Delta IEC}$
	Ki67 Scholzen et al. - 2000 Lawless et al. - 2010	✓	✗	✗	✗
	γH2A.X Collado et al. - 2007 Lawless et al. - 2010	✗	—	✓	✓
	p21$^{WAF1/Cip1}$ Collado et al. - 2007 Demidenko et al. - 2008	✗	✗	✓	✓
	p16^{INK4A} Kiulmann et al. - 2010	✗	✗	✓	✓
	SA-β-Gal Severino et al. - 2000 Debacq-Chainiaux et al. - 2009	✗	✗	✓	✓
	G1 cyclins Blagosklonny et al. - 2006 Pejalunga et al. - 2007	✓	✗	✓	✓

NOTE. Typical profile of proliferation, quiescence, and cellular senescence are shown. VEGFR2 mice showed a phenotype highly resembling cellular senescence.

Supplementary Table 2. Clinical Data of Patients Examined in Figure 7

Patient ID	age [y]	gender	histology	grading	UICC	RECIST	progression?	PFS [m]	alive?	OS [m]	ΔSenescence
SF001	25	f	adenocarcinoma	2	IV	CR	n	16,6	n	16,6	HI
SF002	45	f	adenocarcinoma	3	IV	PR	y	19,3	n	21,3	LO
SF003	55	m	adenocarcinoma	3	IV	PR	n	45,0	y	45,0	HI
SF004	60	m	adenocarcinoma	3	IV	SD	n	20,0	y	20,0	HI
SF005	70	m	adenocarcinoma	2	IV	PD	y	1,6	y	43,2	LO
SF006	21	f	adenocarcinoma	3	IV	SD	y	5,9	n	8,3	LO
SF007	68	m	adenocarcinoma	2	IV	PR	y	41,7	y	87,2	LO
SF008	66	f	adenocarcinoma	2	IV	PR	n	21,9	y	21,9	HI
SF009	62	m	adenocarcinoma	2	IV	CR	n	29,1	y	29,1	HI
SF010	48	m	adenocarcinoma	2	IV	SD	y	6,3	n	38,1	LO
SF011	54	m	adenocarcinoma	2	IV	SD	n	13,5	n	13,5	LO
SF012	71	m	adenocarcinoma	2	IV	SD	y	4,1	y	43,4	HI
SF013	70	m	adenocarcinoma	3	IV	SD	y	10,1	y	31,4	LO
SF014	36	f	adenocarcinoma	3	IV	SD	y	4,1	n	17,0	LO
SF015	65	f	Signet ring cell carcinoma	3	IV	PR	n	17,4	y	17,4	HI

All data as of 10/2013

CR, complete remission; OS, overall survival; PD, progressive disease; PFS, progression-free survival; PR, partial remission; RECIST, Response Evaluation Criteria in Solid Tumors; SD, stable disease; UICC, Union Internationale Contre le Cancer (cancer classification).

Supplementary Figure 1. Confirmation of knockout animals and cells. (A) Conditional knockout in IECs of VEGFR2 in mice was confirmed using qPCR. IEC isolation was performed after DSS stimulus. (B) VEGFR2$^{\Delta IEC}$ mice show no spontaneous colonic phenotype as evaluated by endoscopy or histopathology. C-P21 knockout in cells is confirmed by qPCR (n ≥ 4 mice per group; representative of in vivo experiments performed in independent duplicates).
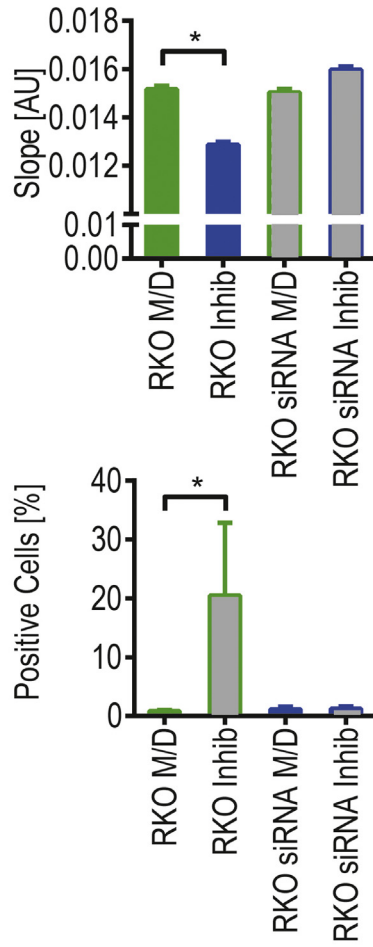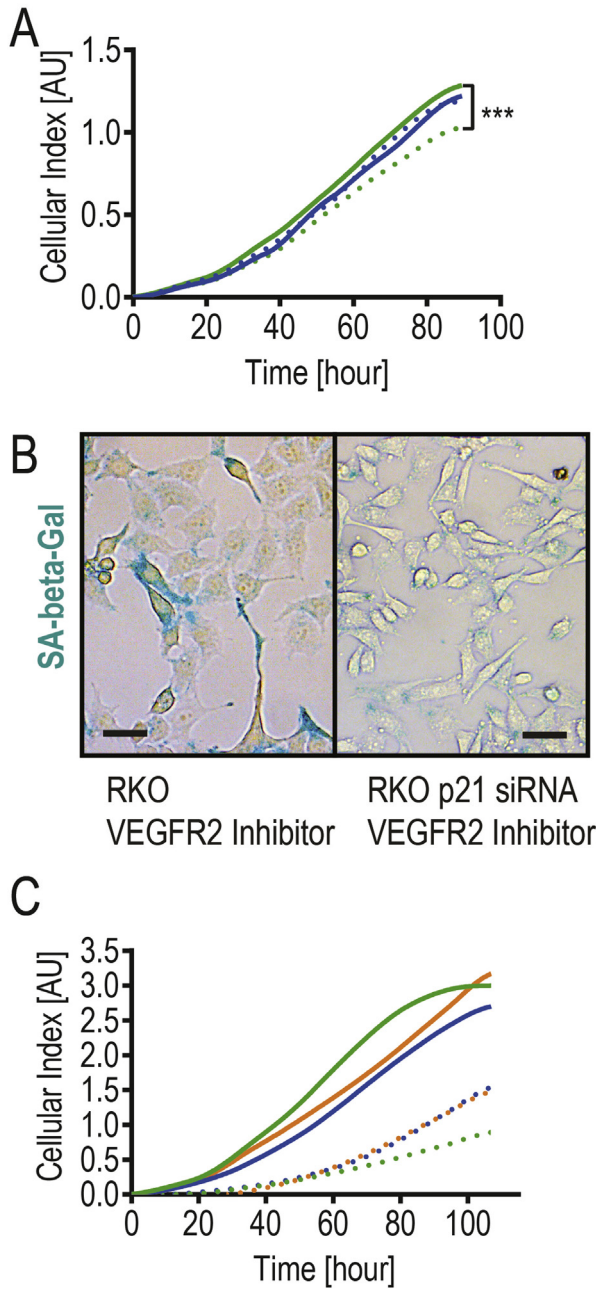
Supplementary Figure 2. Confirmation of in vitro studies with second cell line and small interfering RNA (siRNA) mediated knockdown (similar to Figure 4). (*A*) In vitro dynamic growth monitoring with the xCELLigence system of RKO and RKO + p21 siRNA cells after VEGFR2 inhibition as done corresponding to Figure 4 (RKO control: *solid green*; RKO with inhibitor: *dashed green*; RKO p21 siRNA control: *solid blue*; RKO p21 siRNA with inhibitor: *dashed blue*). Growth curves and slopes were compared (*upper panel*). Quantification of cellular senescence as detected by Sen-β-Gal and positive cell count (*lower panel*). (*C*) XCELLigence growth monitoring in HCT116[wt] (*green*), HCT116[p21−/−] (*blue*) and HCT116[p53−/−] (*orange*) cells after AKT inhibition (medium/dimethyl sulfoxide: *solid line*, inhibitor: *dashed line*).
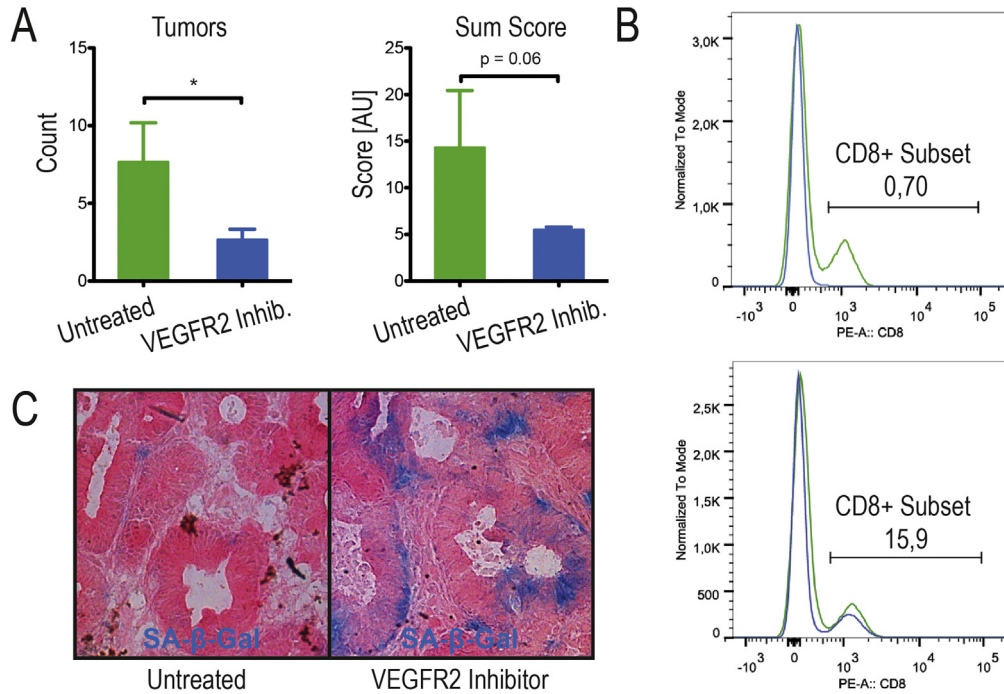
Supplementary Figure 3. Preparatory experiments to Figure 6. (*A*) Treatment of C57BL/6 mice with VEGFR2 inhibitor was compared with untreated animals using endoscopic scoring of the tumor burden (sum score) and the tumor count. (*B*) Induction of cellular senescence upon treatment was evaluated using Sen-β-Gal. (*C*) Depletion of CD8$^+$ T cells was confirmed by fluorescence-activated cell sorting (FACS) analysis. FACS analysis after intraperitoneal injection of the depletion antibody (*green curve*) led to a >90% reduction of CD8$^+$ T cells when compared with the value before application (*blue curve*). (*E*) This depletion lasted well until the next application every 4 days as confirmed by FACS analysis. No difference in CD8$^+$ T-cell count was observed in untreated animals (n $\geq$ 4 mice per group).
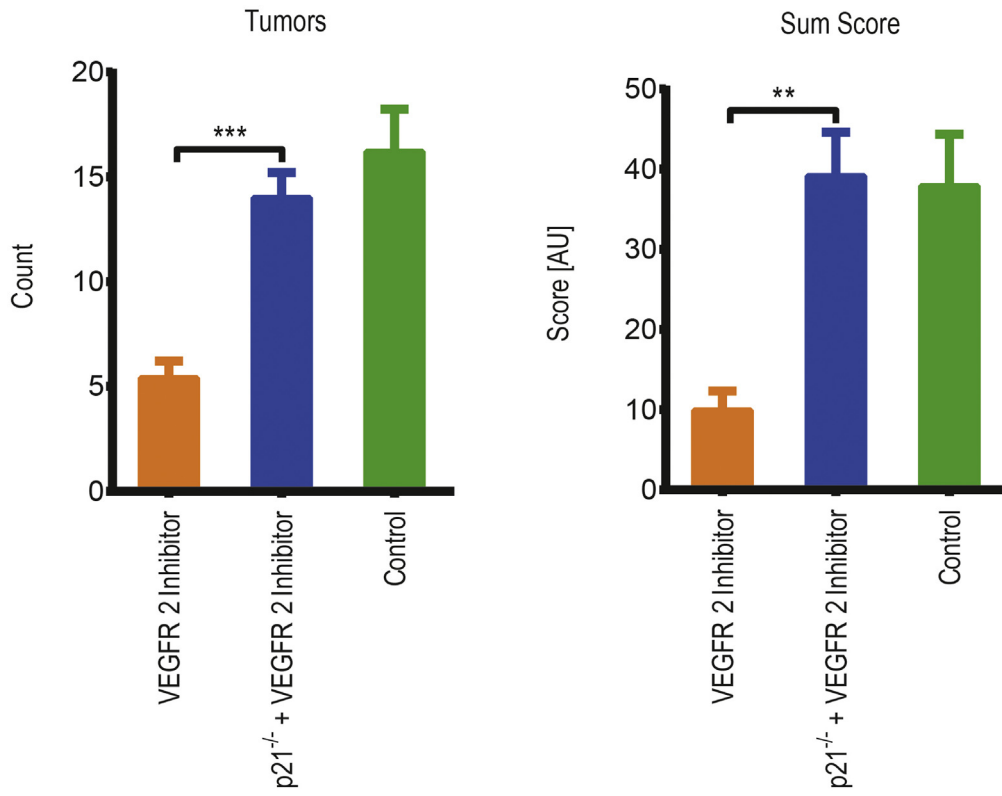
Supplementary Figure 4. VEGFR2 inhibition in p21$^{-/-}$ mice. Tumor count and burden was assessed in control mice, wild-type mice receiving VEGFR2 inhibitor and p21-deficient mice receiving VEGFR2 inhibitor (n $\geq$ 5 mice per group).
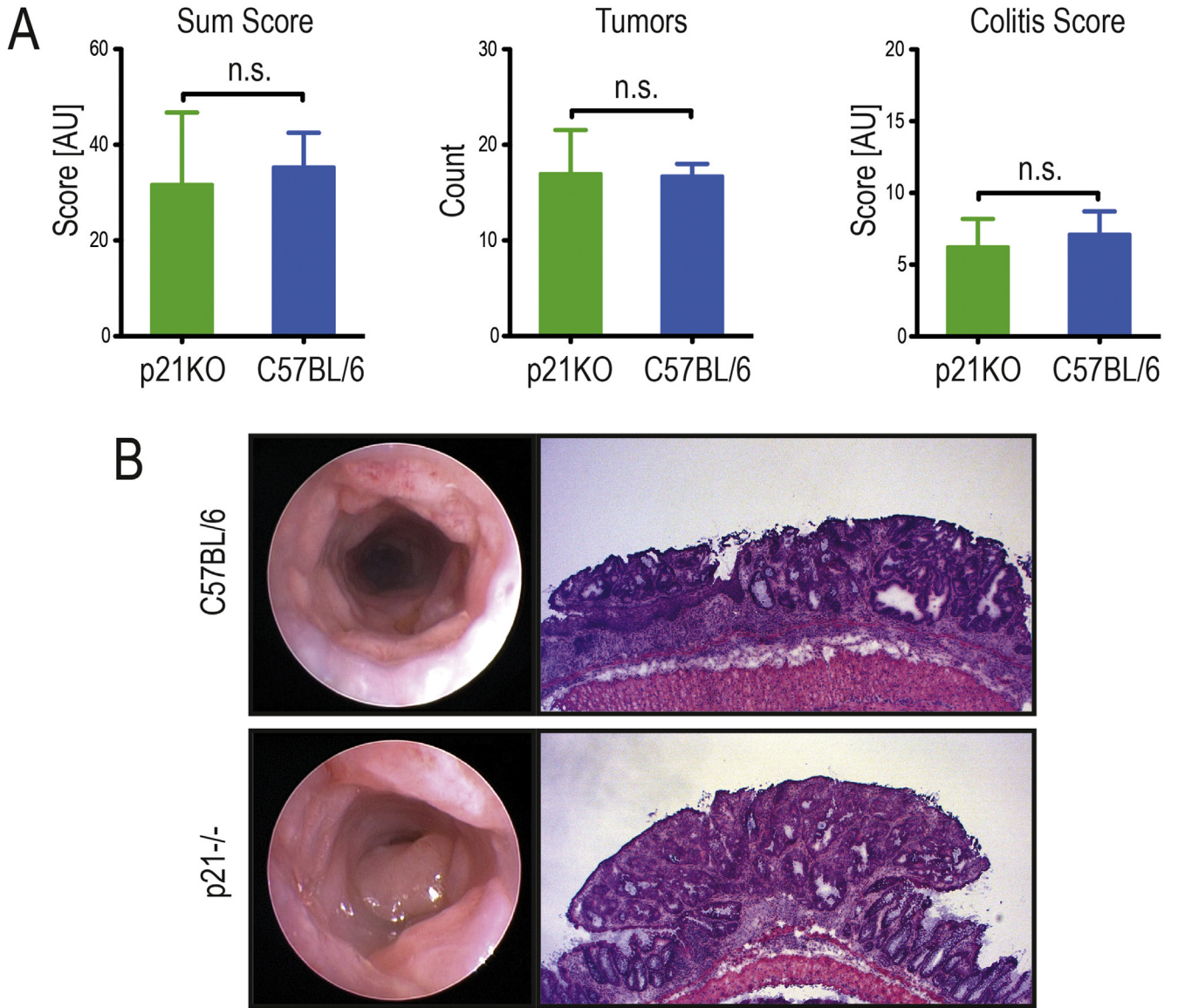
Supplementary Figure 5. p21-deficient and wild-type mice in CAC. (*A*) There was no significant difference in CAC development after AOM injection and DSS-induced colitis, when p21-knockout and wild-type mice were compared. This holds true for tumor burden, tumor count as well as colitis scoring. (*B*) Representative endoscopic and H&E images of colorectal tumor development (n $\geq$ 4 mice per group).
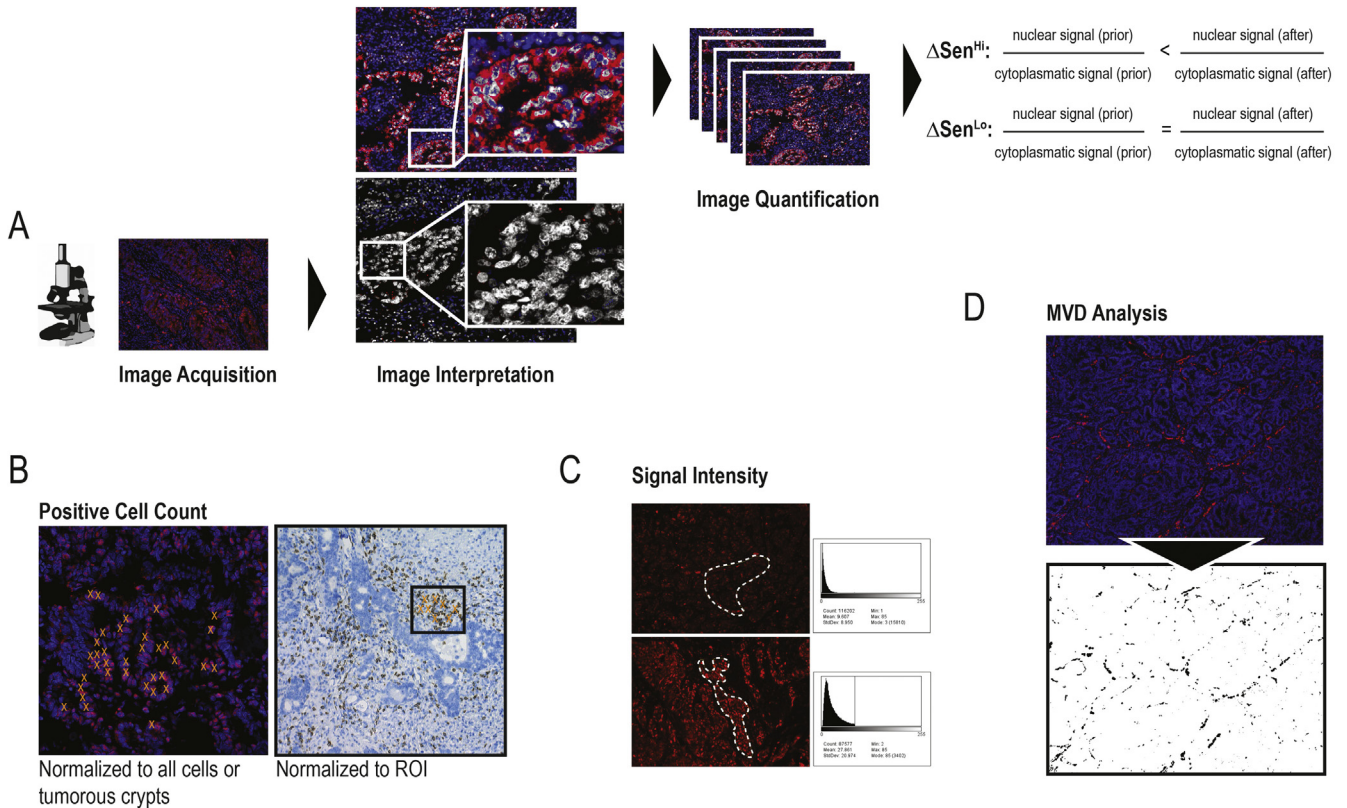
Supplementary Figure 6. Image analysis used in this study. (*A*) To group patients according to p21-modification/inactivation before and after bevacizumab treatment, immunohistochemistry was performed. Same staining protocols and imaging parameters (exposure, etc) were used during image acquisition. Overlay of *blue* and *red* channel is shown in *gray* false color for better distinction. Cells with a predominantly nuclear or cytoplasmatic staining were counted in 3−5 representative images per patient before and after treatment (n = 15 patients/30 samples). Patients were then grouped into ΔSenescence^{Hi} (>10% shift from cytoplasmatic to nuclear p21) and ΔSenescence^{Lo} (<10% shift from cytoplasmatic to nuclear p21 or shift from nuclear to cytoplasmatic p21) according to the difference in these ratios. (*B*) Positive cells were counted per longitudinal crypt, tumorous crypt, or region of interest (ROI) and whenever applicable normalized to total number of DAPI-positive cells. (*C*) Signal intensity was calculated by analyzing mean signal values of similar ROIs. (*D*) MVD was calculated by first extracting information about vasculature from CD31 staining and then analyzing the positive particles per mm^2.
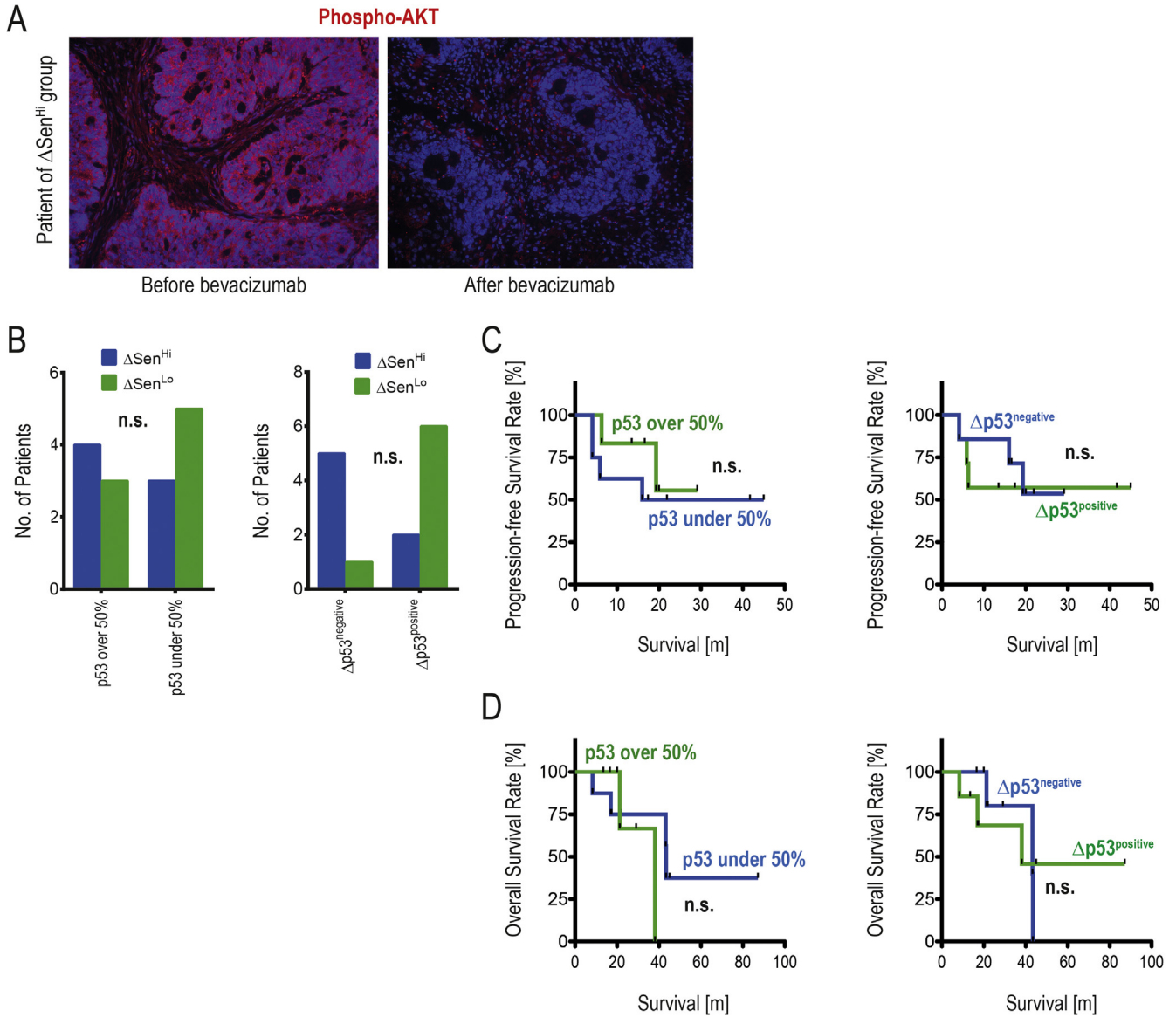
Supplementary Figure 7. Additional information on patient cohort. (*A*) Representative image of phosphorylated (activated) AKT before and after bevacizumab treatment in a patient in the ΔSenescence^{Hi} group (n = 4 patients/8 samples were investigated). (*B*) P53 status was evaluated using routine pathologic IHC. Approximate percentages of p53-positive tumor cells as well as semi-quantitative signal intensity (0−3) were examined. Bar charts of ΔSenescence^{Hi} and ΔSenescence^{Lo} patients are shown according to the percentage of p53-positive cells (*left*) and the change in p53-positive cells during treatment (*right*). Fisher's exact test was used to calculate correlation, which did not reach statistical significance (n = 14 patients/26 samples). (*C, D*) Kaplan-Meier-Curves depicting progression-free and overall survival are shown for both initial p53-positive cell percentage (*C*) and change in p53 positivity during therapy (*D*).